INTERNATIONAL JOURNAL OF
COASTAL, OFFSHORE & ENVIRONMENTAL ENGINEERING IJCOE Vol.8/No. 1/winter 2023 (45-60)

Available online at: www. Ijcoe.org

Experimental and Numerical Investigation of Degree of Freedom Effects on Hydrodynamic Performance of Floating Breakwaters Under Regular Waves

Naser Abasi [1], Cyrus Ershadi [2*], Mohamad Ali Lotfollahi Yaghin [3], Alireza Mojtahedi [4]

[1] *PhD. in marine engineering, University of Hormozgan; N.Abasi.Phd@hormozgan.ac.ir*
[2*] *Assistant professor, University of Hormozgan; Cyrusershadi1@yahoo.co.uk*
[3] *Professors, University of Tabriz; Lotfollahi@tabrizu.ac.ir*
[4] *Associate professor, University of Tabriz; A.Mojtahed@tabrizu.ac.ir*

ARTICLE INFO

Article History:
Received: 05 Sep. 2022
Accepted: 28. Jan 2023

Keywords:
Floating Breakwater
Degree of Freedom
Stiffness of Anchorage System
Hydrodynamic Performance
Transmission Coefficient

ABSTRACT

In designing of any system that deals with forces and displacements some of the effective parameters on hydrodynamic behavior that needs to be investigated are the degree of freedom, and the stiffness of the support systems. In the present study, the effects of degree of freedom on hydrodynamic performance of a box type floating breakwaters (FB) is investigated experimentally and numerically. The experiments were conducted in the 2D wave flume of the (SCWMRI). Regular waves were generated by a piston type wave paddle controlled by 'DHI wave generating' software. The effect of incident waves characteristics on efficiency of FB is examined in four configurations. In this paper, a new dimensionless parameter (DB/L^2, i.e., draft times width divided by wavelength squared) is identified as an essential parameter for comparison between theories and the experimental data. Generally, the most efficient configuration is the fixed breakwater, but considering the tidal phenomenon, providing the required draft of FB will increase the cost of project. For short wavelengths, it is seen that the efficiency of pile-restrained FB is good same as the fixed type in mild conditions. Regarding the cost-effectiveness, the configuration of the FB with the pile should be considered the most efficient for design purposes in mild conditions.

1. Introduction

With the increasing importance of port construction economics, one of the most useful possible options can be floating breakwaters. Moreover, they have less damage to coastal ecosystem. The safety of these structures under wave action is of utmost importance to avoid significant economic losses, and negative environmental and social impacts. A conventional solution for protecting marine structures and fragile shorelines is to use bottom-founded breakwaters which can be constructed by using quarried rocks or concrete caissons resting on a foundation on the seabed. While the bottom-founded breakwater solution is effective in blocking ocean waves, it may not be economical for water depths larger than 6m or for soft seabed due to the enormous foundation costs [1]. The importance of this issue is doubled when the mild wave conditions become dominant in the port location. Nowadays, the use of floating breakwaters is increasing, so more research is needed to expand human knowledge about their hydrodynamic behaviors. Floating breakwaters have many benefits, including low running costs, no dependence on seabed soil characteristics, and rapid installation and operation but the main problem with them is their low efficiency against long waves. Floating breakwaters (FBs), compared with the traditional fixed-bottom breakwaters, are less dependent on the bottom topography and seabed conditions, they are more economical, and they can be easily installed, assembled, and removed. Furthermore, floating breakwaters are eco-friendly. Therefore, this type of breakwaters has been considered by researchers and a lot of studies have been done on them in recent decades (Abul-Azm and Gersha; Carr; Duan et al.; Weng and Chou).

Dai et al, classified FBs into seven categories according to their shapes: (1) box-type, (2) pontoon-type, (3) frame-type, (4) mat-type, (5) tethered float type, (6) horizontal plate type, and (7) other types. Since the shape of the structure affects the mechanism of wave energy dissipation, it is an important parameter for its efficiency. In addition to the shape of the structure, the

type of structural restraint system also affects the hydrodynamic performance of the structure. FBs have been investigated in three modes namely, fixed breakwaters (no degree of freedom), FBs restrained by pile (1 degree of freedom) and FBs restrained by mooring lines (6 degree of freedom). Moored FBs can have different hydrodynamic performance depending on the length, stiffness, and angle of mooring lines.

Carr developed an equation for the transmission coefficient of a rectangular cross-section assuming linear damping. The solution was introduced for shallow water waves; hence the pressure distribution was hydrostatic [26].

1.1. Experimental studies

Koutandos et al. studied a fixed and pile-restrained box-type FB experimentally and explored the effect of attaching a plate to the structure. They concluded that the heave motion FB operated in a dissipative manner, with much lower reflection than that of the single fixed breakwater. Also, a numerical and experimental investigation was conducted by Koutandos and Prinos, [4].

In the mentioned study, the wave interaction with a fixed, partially immersed breakwater of box type with a plate attached (impermeable–permeable) to the front part of the structure was investigated. Based on the hydrodynamic characteristics, it was inferred that the breakwater with an impermeable plate attached to its bottom is more efficient. The comparison of horizontal and vertical forces acting on the breakwater for all cases examined reveals that the plate porosity influences slightly the vertical force and severely the horizontal force acting on the structure, reducing maximum values in both cases.

Tolba investigated experimentally the effect of the draft and width of the fixed box-type breakwater. The results illustrated that, with increasing the draft and width of the structure, the transmission coefficient decreased. Also, Tolba and Isaacson and Bhat studied experimentally the influence of the heave motion on the efficiency of the pile-restrained FBs and. Ruol et al. studied the effect of mooring stiffness on the behavior of π-type FB experimentally and numerically. They compared FB anchored by pile, tethered with elastic lines and loose chain. The results concluded that the most effective restraining system depended on the range of periods and the ratio between draft and depth. The performance of the FBs moored with tethered lines was better than that of the FBs moored with loose chains. For periods shorter than the natural period of FB, pile supported FBs performed better than tethered supported ones. Also, for periods close to the natural period of FB, chain moored FBs behaved better than pile supported FBs.

Ruol et al. developed a modification factor for the formula of Macagno to approximate the wave transmission coefficients of floating breakwaters anchored by chains or cables. This modification factor is based on a dataset of experimental data, and it is a function of the relative period χ which is defined as the wave peak period over the natural heave period (T_p/T_h). Based on examination of the applicability of this formula, it is concluded that this formula is valid for ordinary pontoon type and π-type floating breakwaters anchored by chains. Furthermore, the formula is valid for a relative draft (D/d) range between 0.20 and 0.60 and for relative period range ($T_p/T_h = \chi$) between 0.50 and 1.50. The dimensionless parameter χ is determined as follows [5]:

$$\chi = {T_p}/{T_h} = \frac{T_p}{2\pi}\sqrt{\frac{g}{D+0.35B}} \quad (1)$$

where g is acceleration due to gravity, D is the draft, d denoted the water depth and B is the FB's width. Ruol considered the peak period T_p (irregular waves), but Macagno assumes mean period T_m in his theory (only regular waves), hence, to apply Macagno in combination with χ, the wave period T_m for the calculation of χ should be increased by 10%.

Peña et al. investigated wave transmission coefficient experimentally, mooring lines with four different configurations of FBs. A comparison of elastomeric mooring versus chains was made. Results revealed that with the elastic mooring lines, the static loads were greater, but the dynamic ones were lower. Also, the mooring lines configuration had no influence on the wave transmission [9].

Yamamoto investigated a rectangular cross-section and a hydrodynamically shaped 'three-cycle cylinder' breakwater. The results showed that the dynamic mooring force in the sea-side line was considerably larger than that in the leeside [28].

Ning et al. examined and introduced a pile-restrained WEC-type floating breakwater. Vertical piles prevent horizontal movement and permit only the heave motion. However, the pile restrained FB is relatively expensive. In addition, it has some disadvantages such as strong abrasion between structure and pile, withstanding large wave loads and not being suitable for deep water and poor foundation [1].

Ozeren et al. setup a laboratory investigation of the hydrodynamic interaction of cylindrical breakwaters with monochromatic waves in deep and transmissional water depths. Results showed that, when the breakwater models were fixed, the reflection was higher than the partially restrained models, and the efficiency was strongly dependent on draft ratio (z_d/d, where z_d is the draft and d represent the height of the structure).

For the measured range of waves, z_d/d=0.7 was the best value of the tested draft ratios for the pile-restrained model and horizontal restraint was found to be more important than vertical restraint in terms of improving the breakwater efficiency.

Veldee showed that in any ratio of wavelength to breakwater length, with increasing wave height, the mooring force also increased. Ji et al. setup a 2D experiment to study four models; including a traditional box-type FB, namely the traditional cylindrical FB, the cylindrical FB with cage and the cylindrical FB with cage and suspended balls. They concluded that mooring forces increased with the wave period for all four models. Forces acting on the windward mooring lines of the cylindrical model with cage and suspended balls were at least 50% larger than the other two cylindrical models [21]. An experimental study of a porous floating breakwater was carried out by Wang and Sun. They considered two mooring modes; directional mooring, and bidirectional mooring. They concluded that the transmission coefficient of the bidirectional mooring declined 20% by comparing it with the directional mooring. Loukogeorgaki et al. set up an experimental investigation by a 3D physical model focusing on the structural response (connector and mooring line loads) for assessing the wave attenuation effectiveness of a FB, consisting of an array of multiple floating box-type modules, under the action of perpendicular and oblique regular and irregular waves. They concluded that the FB's structural response depends strongly upon the wave period, while the wave height and the angle affect this response mainly in the low frequency range. The increase of the wave obliqueness may lead to a more efficient FB in terms of both functional and structural integrity issues.

1.2. Numerical studies

Zhang et al. used the CFD method to simulate the hydrodynamic properties and the vorticity characteristics of a fixed rectangular, inverted π-type and L-type breakwater. The numerical accuracy of the viscous model is confirmed by comparison of the wave transmission and reflection coefficients between the viscous flow, potential flow, and experimental results. Furthermore, the vorticity field on these two types of FBs are discussed and compared respectively. Further, the characteristics like the vortex evolution, the flow pattern, and the vorticity magnitude around the inverted π-type fixed breakwater is analyzed in detail. They proposed the L type breakwater and showed that this model had a better performance than the other two models.

Using a theoretical and numerical study, Drimer et al. investigated a box-type FB with various mooring stiffness. The implementation of simplifying assumptions concerning the flow beneath a pontoon-type floating breakwater leads to an analytical solution of the two-dimensional linearized hydrodynamic problem. They suggested a flexible mooring system, which reacted to the drift force only, was a more practical solution for large structures [1]. Gesraha investigated the reflection and transmission of incident irregular waves interacting with a π-type floating breakwater using an eigenfunction expansion method [15].

Chen et al. studied theoretically the hydrodynamic behaviors of a floating breakwater consisting of a rectangular pontoon and horizontal plates. They concluded that the mooring force of the floating breakwater with plate was less than that of the single pontoon floating breakwater.

Ouyang et al. investigated Bragg reflection from a train of fixed breakwaters. A numerical model of boundary discretization type was developed to calculate the wave field. The results showed that the Bragg reflection exhibited significant dependence on the relative spacing between the breakwaters. Since fixed breakwaters in areas with tides require a lot of materials and as a result have no economic justification, it is preferred to use pile-restrained FBs rather than fixed ones in these areas. The performance of a floating breakwater with cage aquaculture was investigated by Tang et al. using numerical wave tank. They studied the influences of net depth and net width on the dynamic response. The results revealed that the mooring force decreased as the net depth increased, especially in the vicinity of the resonant frequency.

It is obvious that most of the research on floating breakwaters is investigated by two-dimensional models. Furthermore, a comparative review of 3D basin experiment against 2D wave flume experiment can make this fact clear that 3D experiments can obtain more affecting parameters on FB's dynamic characteristics and wave dissipation mechanism. However, prior to finding a remarkable solution in 3D environment, it is necessary to have a better understanding of hydrodynamic behavior in 2D experiments and recognizing most effectual parameters in this regard. The aim of this study is to present a comprehensive study of box-type floating breakwater anchorage systems. For this purpose, a box-type FB is investigated experimentally and numerically in four modes of restrains, which are fixed, pile-restrained, moored by loose chains and tethered by cables. The experiments are conducted under regular waves with different wave heights and wave periods.

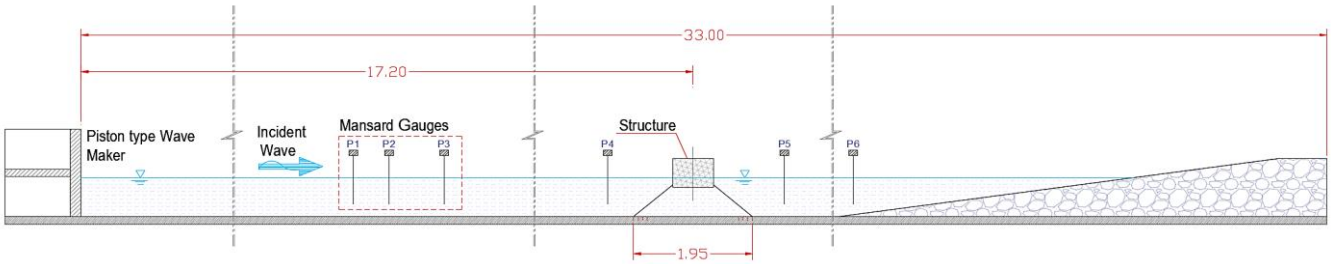

Figure 1. Side view of wave flume and wave gauges position

2. Experimental and numerical procedures

2.1. Experimental setup and test conditions

The experiments were conducted in a 2D wave flume of the research institute (SCWMRI), located in Tehran, Iran. The length, depth and width of the flume were 33*m*, 1*m* and 1*m* respectively. A piston-type wavemaker (made by DHI) was installed at the end of the flume (Figure 3.d) and a wave absorbing beach was located at the other side to prevent the reflection of transmitted waves. The floating breakwater was located 17*m* away from the wavemaker. Figure 1 shows a general layout of the wave flume.

A rectangular box was chosen as the floating breakwater because a lot of research have been done with the mentioned shape. the main geometric parameters of the physical model are presented in Figure 2. where *B* is width of the model, *d* represents water depth and *D* is the draft. Three different drafts of the floating breakwater are implemented in the present study (*D/d*=0.20, *D/d*=0.25, and *D/d*=0.40). To summarize the results, all the results are shown for the relative draft of *D/d*=0.2.

Mansard wave gauges were used to separate the incident and reflected waves. The water depth was 0.67m and the bed was completely flat through the flume length. An absorbing beach in the rear side was used to dissipate the transmitted energy. Several regular waves were generated with different periods and different wave steepness. Resistance type wave gauges (made by DHI) were used for gathering data with sampling frequency of 10*Hz* (Figure 3.a). To calculate the displacement of the floating breakwater, ship movement gages made by DHI Company were used (Figure 3.c). The movement in these experiments were in three directions, heave, sway, and roll. Also,

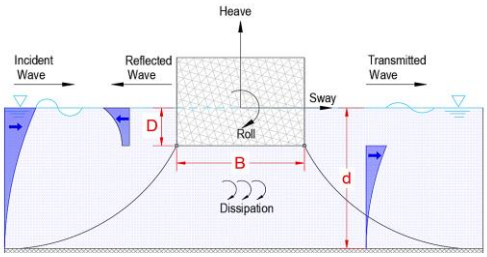

Figure 2. Main geometric parameters of the physical model

the loads on the mooring system were measured by four strain gauges with sampling frequency of 100*Hz*. A pressure sensor was attached on the submerged part of the breakwater in front of the generated waves.

Figure 3. Measurement equipments of the present investigation; (a): Wave gauges, (b): Data logger, (c): Movement gauge, (d): Wavemaker paddel

Numerous wave heights and periods were generated during the experiments to cover the range of intermediate waters. Table 1 shows the experimental test conditions. In the table, *L* is the wavelength and *H* denotes the wave height.

In this research, the Zero-up crossing method is used to analyze the data recorded by the sensors. The MATLAB software is used to code the mentioned method. An example of regular wave analysis output generated in the laboratory is shown in Figure 4. The WAFO module of MATLAB software also is used to control the distribution of the generated waves. The normal probability distribution as well as the up-crossing intensity diagram for the waves are plotted in

Table 1. Experimental test conditions

CONFIGURATION	H(*m*)	T(*s*)	L(*m*)	D(*m*)	D/d	B(*m*)	B/L	T_H
Fixed	0.07-0.1	0.70-4.20	0.77-10.5	0.13-0.27	0.20-0.40	0.67	0.064-0.87	1.22-1.35
Pile-restrained	0.07-0.1	0.70-4.20	0.77-10.5	0.13-0.27	0.20-0.40	0.67	0.064-0.87	1.22-1.35
Anchored by chain	0.07-0.1	1.00-4.20	1.55-10.5	0.13-0.27	0.20-0.40	0.67	0.43-0.87	1.22-1.35
Tethered by cable	0.07-0.1	1.00-4.20	1.55-10.5	0.13-0.27	0.20-0.40	0.67	0.43-0.87	1.22-1.35

Figure 5 to examine the generated waves degree of similarity with the Gaussian Sea waves (in this figure the number of up-crossings of wave data is plotted and compared with an estimation based on the assumption that the data is a realization of a Gaussian Sea).

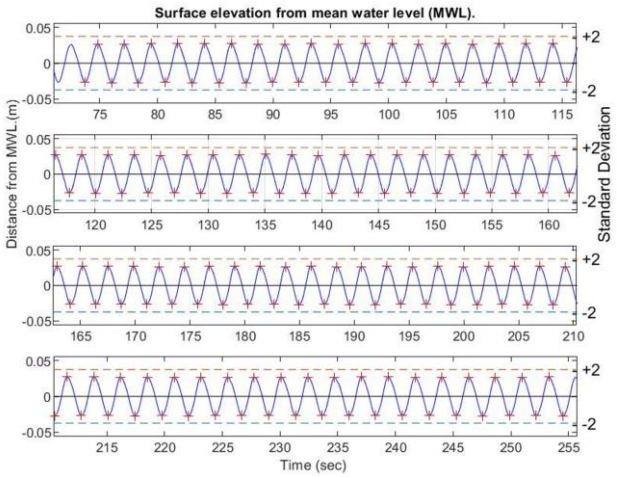

Figure 4. A sample of regular wave analysis output generated in the laboratory

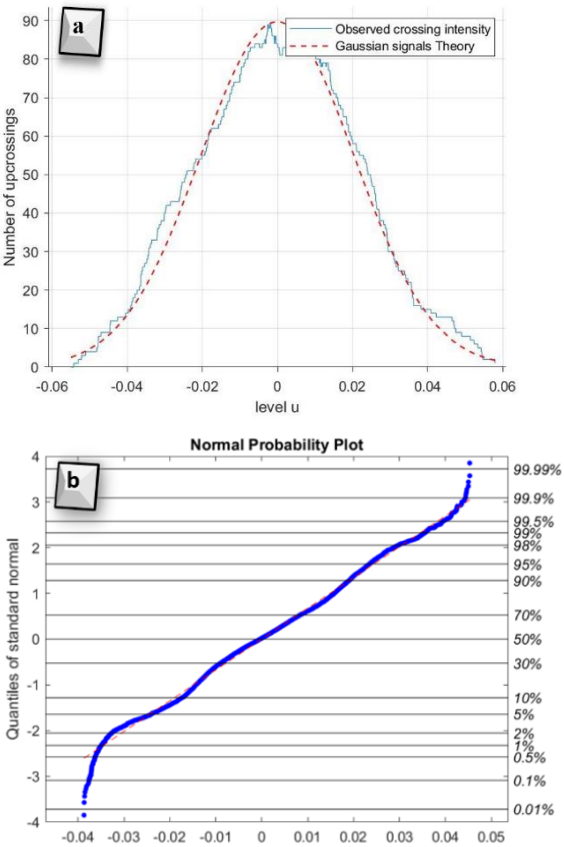

Figure 5. (a): Up-crossing intensity diagram, (b): Normal probability distribution

In the case of the pile-restrained model, the desired drafts were provided by attaching extra weights to the physical model. These extra weights were distributed uniformly on the model's mass point level. To provide feasible movement of the structure in the heave direction, two iron rails were attached to the flume walls (Figure 6). The mentioned rails restrained horizontal and rotational motions and the model was only allowed to have motion in the heave direction with minimum friction. All of the movement gauges were calibrated before use.

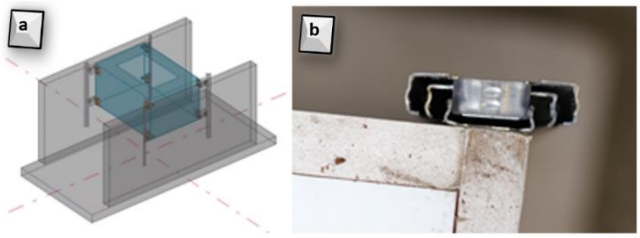

Figure 6. Provided supports for the fixed and pile-restrained FB; (a): Fixed Breakwater 3D model, (b): Iron rails cross section

In the case of the model with mooring lines, four cables (or chains) were connected to the submerged part of the model and on the other side, they were hooked to the bed of the flume with the angle of 45 degrees (Figure 7). The length of the cables were adjusted so that the desired drafts were achieved, and the cables were always in a state of tension simultaneously. Chains were in loose condition and had submerged weight of 259 *g/m* and the length was 3.35*m*, i.e., five times the water depth. The initial mooring stiffness was low, and no shocks were observed during the experimental tests.

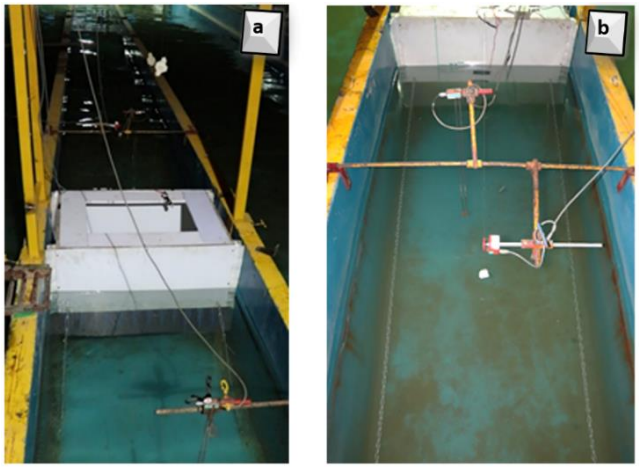

Figure 7. Provided mooring lines for the physical model; (a): Model with tethered cable, (b): Model with loose chain

Figure 8. The installed physical model in the wave flume;
(a): Anchored by cable, (b): Fixed Breakwater, (c): Anchored by chain.

The model was 0.67m in width and 0.50m in height. The length of the model was approximately equal to the flume width. To avoid unnecessary friction or collisions between the walls and the physical model, a gap was provided between the model and the walls. Also, for restricting wave transmission through the mentioned gap, some flexible polystyrene sheets were attached to the floating breakwater. The installed model is shown in Figure 8.

2.2. Data acquisition and analysis

Wave reflection and transmission were estimated for every case. A three-point method, proposed by Mansard and Funke, was employed to separate incident waves from reflected waves [3]. Six resistance wave gages made by DHI Denmark were used along the wave flume surrounding the structure to record the wave profile. Four of them were placed in the seaside of the model and two gauges were placed in the leeside. The transmission and reflection coefficients are calculated according to equations (2) and (3), respectively [20].

$$C_t = \frac{H_t}{H_i} \tag{2}$$

$$C_r = \frac{H_r}{H_i} \tag{3}$$

where H_t is the transmitted wave height, H_r represents the reflected wave height and H_i denotes the incident wave height. The transmission coefficient (C_t), the reflection coefficient (C_r), and the dissipation coefficient (C_d) satisfy equation (4). Using the following equation energy dissipation was studied in floating breakwater's region [4].

$$C_r^2 + C_t^2 + C_d^2 = 1 \tag{4}$$

The motion responses of the floating breakwater were measured by ship movement gages which were made by DHI Company. The movement in these experiments were in three directions, heave, surge, and pitch. The heave, surge, and pitch RAOs (Response amplitude operators) were calculated using equations (5)-(7) (He et al. 2013). The data extracted from the gages were analyzed by Wavepack software. Figure 3 shows the gages and the data recording systems.

$$RAO_{surge} = \frac{A_{surge}}{A_i} \tag{5}$$

$$RAO_{heave} = \frac{A_{heave}}{A_i} \tag{6}$$

$$RAO_{pitch} = \frac{A_{pitch}}{A_i} \tag{7}$$

In which, A_{surge}, A_{heave} and A_{pitch} are the amplitude of the surge, heave, and pitch respectively, and Ai is the amplitude of the incident wave.

2.3 The basic FB structures for the numerical analysis

In the present study, a finite-volume software, is applied based on the RANS (Reynolds Averaged Navier-Stokes) equations. RANS coupled with the continuity equation for incompressible flows in Cartesian coordinates are considered as the governing equations as follows [29]:

$$\frac{\partial \rho \overline{u_i}}{\partial x_i} = 0 \tag{8}$$

$$\frac{\partial}{\partial t}(\rho \overline{u_i}) + \frac{\partial}{\partial x_i}\left(\rho \overline{u_i u_j}\right) = -\frac{\partial P}{\partial x_i} + \frac{\partial}{\partial x_i}\left[\mu\left(\left(\frac{\partial \overline{u_i}}{\partial x_j} + \frac{\partial \overline{u_j}}{\partial x_i}\right)\right) - \frac{2}{3}\mu \frac{\partial \overline{u_i}}{\partial x_i}\delta_{ij}\right] + \frac{\partial}{\partial x_j}\left(-\rho \overline{u_i' u_j'}\right) + \rho f_j \tag{9}$$

where $\overline{u_i}$ $\overline{u_j}$ is the time average velocity component, for this 2D simulation, i,j =1,2, represent the horizontal direction of x and the vertical direction of y respectively, P is the pressure intensity, ρ represents the fluid density, f is the unit body force and μ denoted the dynamic viscosity.

Based on the Airy's linear wave theory, the regular wave equation for the free surface elevation $\eta(x,t)$, the velocity potential $\varphi(x,z,t)$, and velocity components in x and z directions $u(x,z,t)$ and $w(x,z,t)$ are written as:

$$\eta = A\cos(kx - \omega t + \phi) \tag{10}$$

$$\varphi(x,z,t) = xU + \frac{A\omega \cosh[K(z+h)]\sin(kx-\omega t+\phi)}{k \sinh kh} \tag{11}$$

$$u(z,x,t) = U + \frac{A\omega \cosh[k(z+h)]\cos(kx-\omega t+\phi)}{\sinh kh} \tag{12}$$

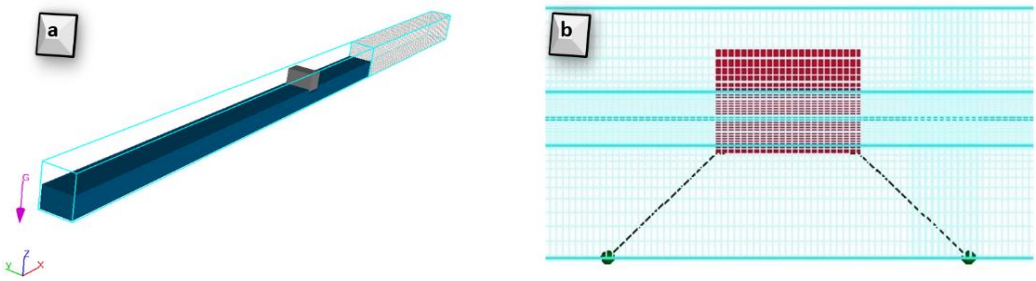

Figure 9. Numerical model computational domain
(a): 3D view of numerical model, (b): Created mesh for simulation

$$w(x,z,t) = \frac{A\omega \sinh[k(z+h)]\sin(kx-\omega t+\phi)}{\sinh kh} \quad (13)$$

in which ω is the angular frequency, k represents the wave number, ϕ is the phase shift angle, h is the water depth and A denotes the wave amplitude. The dispersion equation in terms of wave speed $c = \frac{\omega}{k}$, is given by:

$$(c-U)^2 = \frac{g}{k}\tanh kh \quad (14)$$

In the present study, in order to numerically investigate the effect of the mentioned effective parameters on the hydrodynamic behavior of the floating breakwater, all models of floating breakwaters have been simulated with the application of a finite element software.

The results have been validated with the laboratory data. For numerical modelling, the Cartesian mesh is used in the computational domain. The grid is distributed in the whole computational domain evenly. At the vicinity of the water surface, the mesh densities are increased. The selection of a proper computational mesh is vital in numerical simulations for the solution accuracy and efficiency. Thus, a set of initial numerical simulations were conducted to evaluate the sensitivity of the numerical solutions to the mesh size and an optimum mesh size was obtained. The numerical domain was created in the software. At the left boundary of the computational domain, a numerical wavemaker was established by prescribing the velocities and the free surface elevation according to the linear monochromatic wave. This boundary condition is readily available in the software. The numerical domain is shown in Figure 9. No-slip condition was applied at the bottom and wall boundaries. All numerical wave tanks need to have a dissipation zone to prevent wave reflection and its subsequent problems [30]. A wave absorbing component is installed before an outflow boundary to absorb wave motion, which reduces the wave reflection from the boundary.

The mesh size is one of the important aspects which influences the calculation results. The mesh size relates to the maximum wave frequency which can be calculated by the model. A small mesh size allows high wave frequencies to be calculated. To investigate the effect of the mesh size, several models with the same wave input were made where the mesh size increases from a coarse mesh to a fine mesh. Totally ten calculations were performed to evaluate that whether the results were dependent on the mesh resolution. When the calculation results (C_t) do not change by size decreasing, it can be concluded that convergence has occurred.

2.4. Model calibration and validation

The data of the two-dimensional experiments performed by Koutandos et al. is used to compare for model calibration and validation [4].

In the mesh-independence study, the transmission coefficient at different cell numbers is simulated. The selected wave height is 0.10 m, and the wavelength is 3.35m. The results of the mesh-independence study are shown in Table 2. It is seen that the results are converged to a specific coefficient as the total cells are increased.

Table 2. Mesh-independence test

case	cell number	transmission coefficient
1	1300000	0.635
2	1700000	0.621
3	2000000	0.6113
4	2400000	0.6105
5	2700000	0.6102

3. Results and Discussion

In this section, the results of this investigation are discussed, with emphasis on the effect of the incident wave characteristics, the anchorage systems and draft of the model. In order to compare how well the experimental and numerical results are, the Root Mean Square Error (RMSE) parameter is used:

$$RMSE = \sqrt{\frac{\sum_{i=1}^{N}(Ct_{theory}-Ct_{exp})^2}{N}} \quad (15)$$

where N is the number of data points. RMSE is the standard deviation of the residuals (prediction errors). Residuals are a measure of how far from the regression line data points are; RMSE is a measure of how spread out these residuals are. The difference of the wave transmission coefficient between theories and experimental data is shown in a bar plot to identify

where the largest differences occur. The Root Mean Square Error (RMSE, given in Eq.15) is determined for each theory to see how well the theories behave compared to with the experimental and numerical data. The RMSE applied in this case is a measure of the spread of the experimental data (measured transmission coefficients) and the predicted transmission coefficients (wave transmission theories). The RMSE presents the same units which are used to calculate RMSE, i.e., when the RMSE is calculated with transmission coefficients defined as percentages, the RMSE will indicate the spread of the experimental data around the theories in percentages as well. The plots for each experimental dataset and the RMSE values are given in the following sub-section. Also, the conclusion of each comparison is discussed.

3.1. Anchorage system

The effect of incident waves characteristics, such as wave period and wave heigth, on efficiency is examined in through four different FB configurations: (1) fixed breakwater, (2) pile-restrained (heave motion FB), (3) anchored by chains, and (4) tethered by elastic cable.

3.1.1. Fixed breakwater

Results related to transmission, reflection and dissipation coefficients of the incident waves on the model compared with the other research are presented in Figure 10(a,b,c). Also, a comparative diagram among the experimental dataset, theories and the measured data points are plotted in figure 10-d.

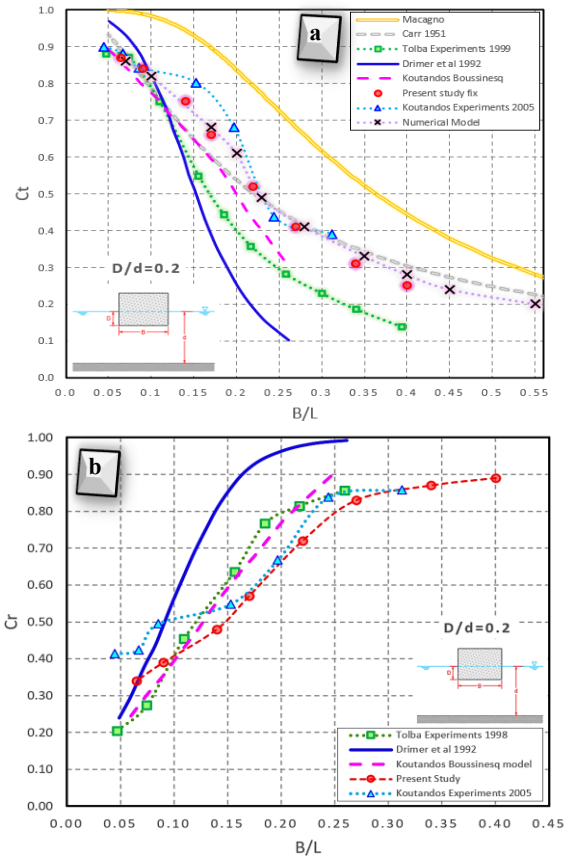

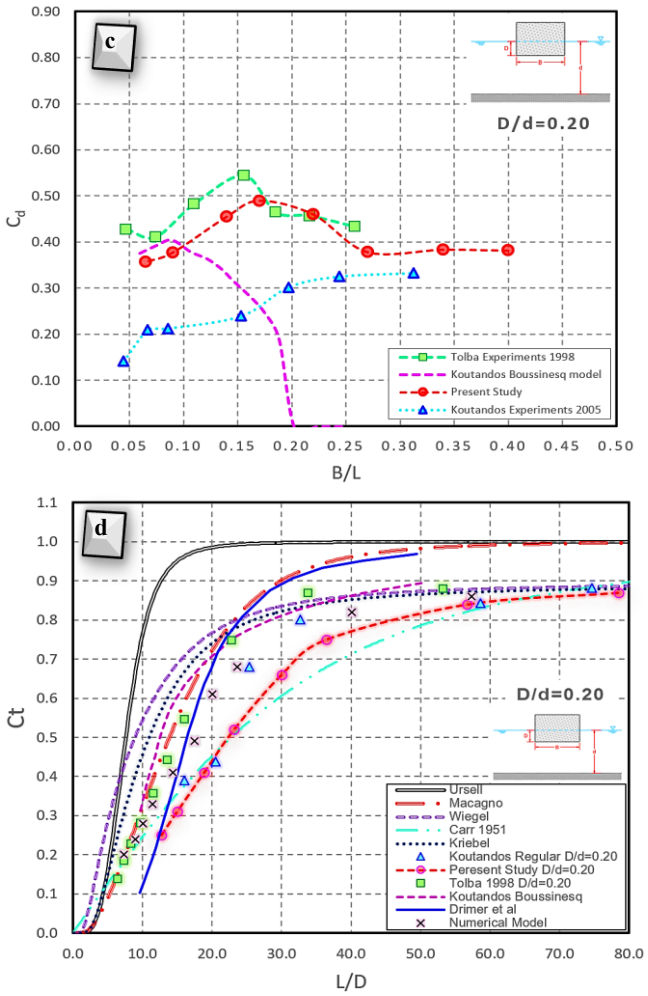

Figure 10. Comparison between theories and the experimental data – For the fixed breakwater;
(a): Variation of transmission coefficient (C_t) against *B/L*
(b): Variation of reflection coefficient (C_r) against *B/L*
(c): Variation of dissipation coefficient (C_d) against *B/L*
(d): Variation of transmission coefficient (C_t) against *L/D*

The difference between theories and the experimental data is shown in Figure 11-b. Also, the Root Mean Square Error (RMSE) for each theory for this dataset is shown in Figure 11-a.

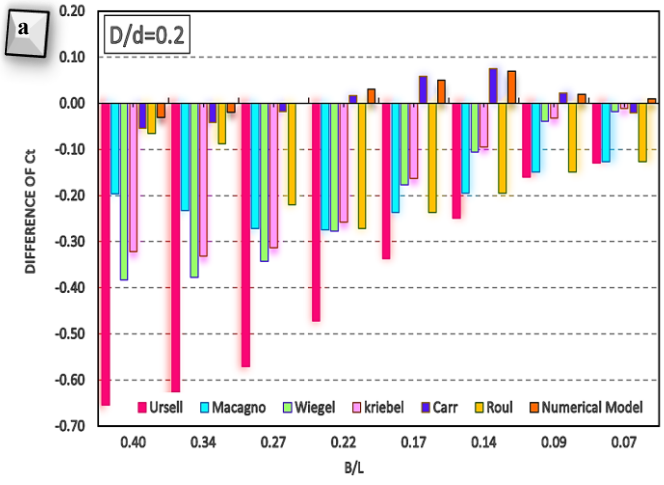

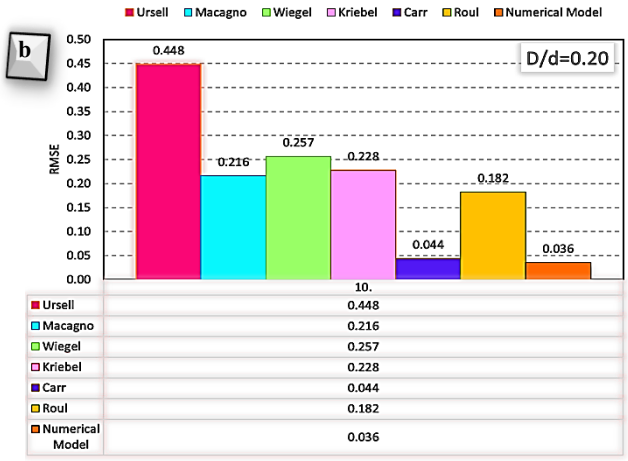

Figure 11. (a): Differences of the C_t between theories and the experimental data,
(b): RMSE between theories and the experimental data in case of the fixed Breakwater

Based on the experimental data obtained from different researchers, several conclusions can be drawn for fixed breakwaters. In general, it can be concluded that the RMSE is large (more than %10) and there is a poor agreement between most of the theories and the experimental data, see Figure 11. The dataset of the present study is overestimated by all of the theories, but Carr formulation has a good agreement with the present data. From this figure and related table, it turns out that the theory of Carr has the smallest RMSE, and this theory might be the most appropriate one to apply for this dataset.

This overestimation becomes larger when the B/L-values increase, hence shorter waves occur. With attention to the large RSME, when the above theories are applied, the wave transmission will be overestimated in general, but for a preliminary design the theories will give a good estimation regarding the effectiveness of the fixed structure. According to the RMSE, a good agreement can be seen between numerical results and experiments of the present study. The RMSE applied regarding numerical model is a measure of the experimental transmission coefficients spread compared with the modelled transmission coefficients by numerical software. On the other hand, results of this study have a good agreement with Koutandos experiments [4].

Based on the present investigation, and with considering the dispersion of laboratory and numerical data obtained from the research on the transmission coefficient, a new non-dimensional parameter (DB/L^2, i.e., draft times width divided by wavelength squared) is identified as an essential parameter to compare all of recent studies. Therefore, it is recommended to use the dimensionless parameter DB/L^2 to compare the transmission coefficient of floating breakwaters. As it can be seen in Figure 12-a (compared with Figure 10-a), the data of different research have a large dispersion, and this is due to the fact that the wavelength parameter (L) has much greater effect than the width of the model (B).

Therefore, in order to have a parameter that can take this effect into account, it is better to use the dimensionless parameter DB/L^2. This parameter brings the existing data to a good consistency and with the convergence that it creates between the data, it helps a lot to understand the results obtained from research with different conditions. An example of this data uniformity for a fixed breakwater under regular waves and D/d=0.2 is shown in Figure 12. In this Figure, data is distributed in a narrow band and there is no much disparity.

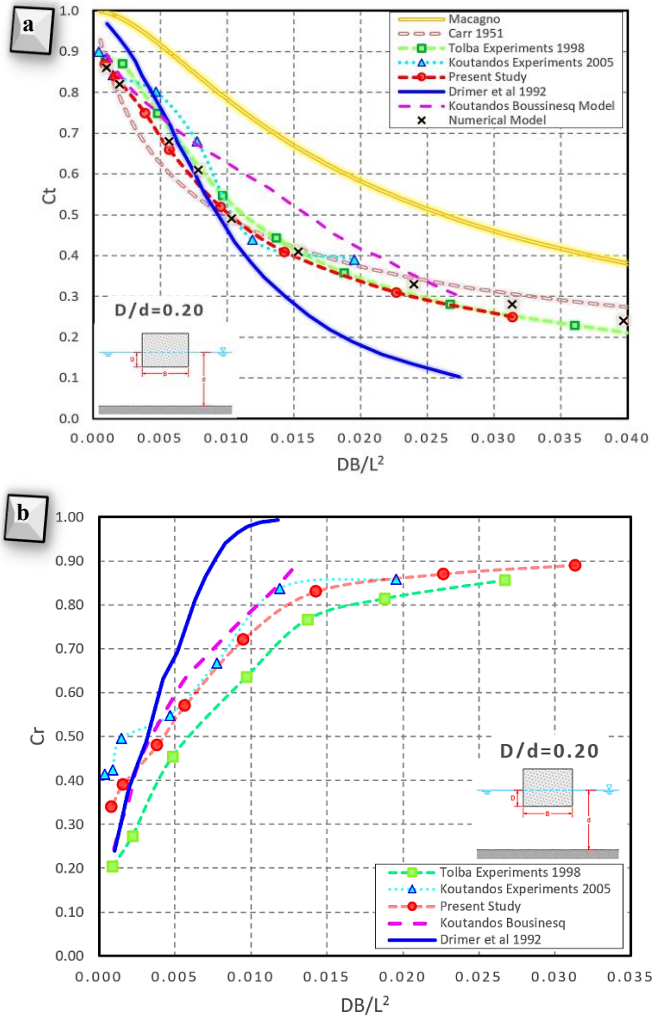

Figure 12: (a): Transmission coefficient (C_t) variation against DB/L^2 parameter, (b): Reflection coefficient (C_r) variation against DB/L^2 parameter – The fixed Breakwater

3.1.2. Pile-restrained floating breakwater

For the FB anchored by pile, the model is free to move just in the heave direction, so it has one degree of freedom. Ruol et al. investigated the natural heave period for pi-type floating breakwaters and compared the analytical calculations with the experimental measurements. Based on this investigation, the dimensionless parameter χ which has been mentioned earlier, is defined in Eq. 1. Therefore, this parameter will be used to set on the x-axis for floating breakwaters

anchored by piles (without fixed vertical screen), because all of the parameters which influence the transmission coefficient are included there [5].

Results related to transmission, reflection, and dissipation coefficients of the incident waves on the model compared with the other research are presented in Figure 13. In this figure, $C_{t,measured}$ represent derived C_t from Macagno formula.

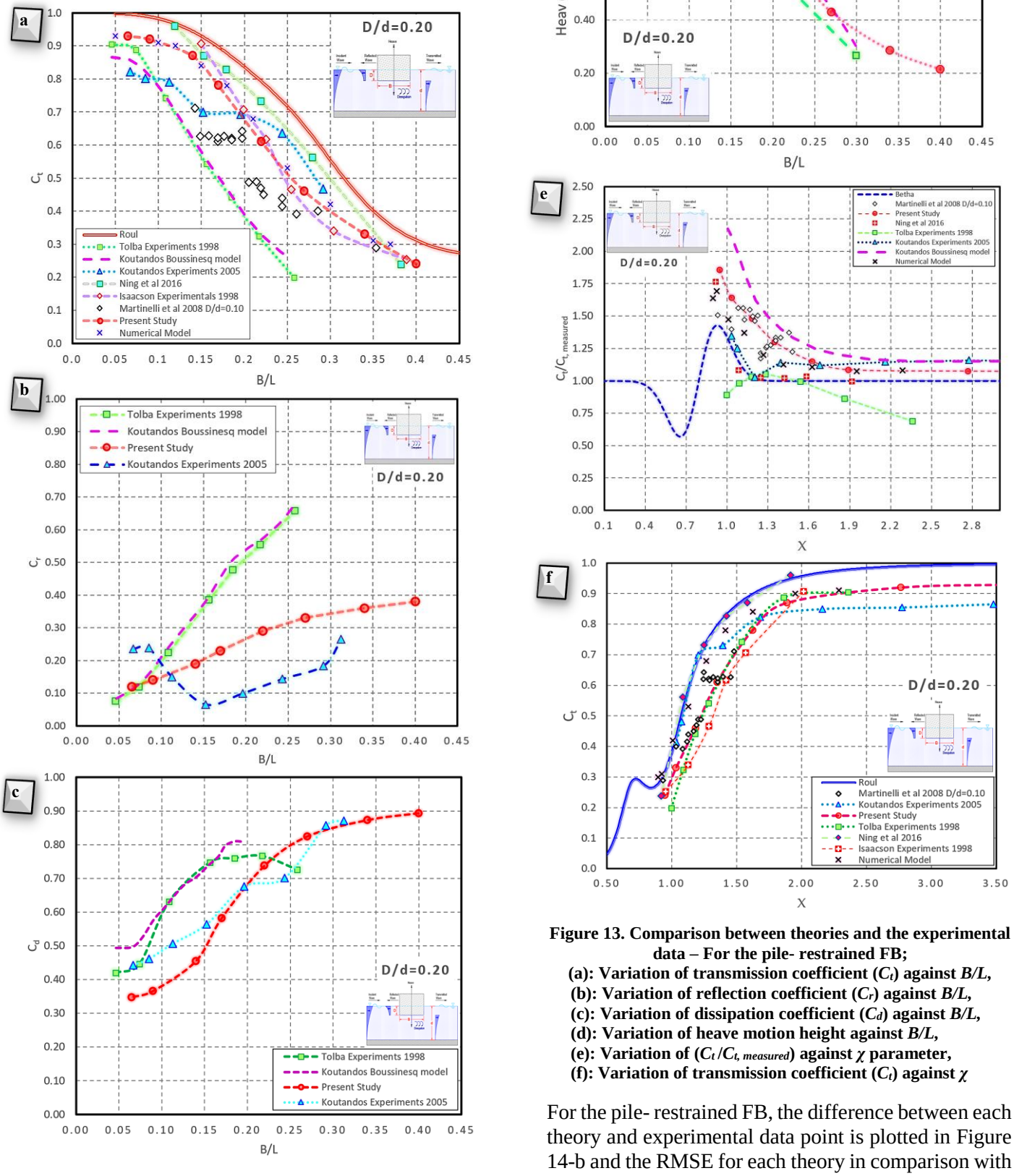

Figure 13. Comparison between theories and the experimental data – For the pile- restrained FB;
(a): Variation of transmission coefficient (C_t) against B/L,
(b): Variation of reflection coefficient (C_r) against B/L,
(c): Variation of dissipation coefficient (C_d) against B/L,
(d): Variation of heave motion height against B/L,
(e): Variation of ($C_t/C_{t,\,measured}$) against χ parameter,
(f): Variation of transmission coefficient (C_t) against χ

For the pile- restrained FB, the difference between each theory and experimental data point is plotted in Figure 14-b and the RMSE for each theory in comparison with this dataset is shown in Figure 14-a. From this figure and related table, the theory of Roul and Carr has the

smallest RMSE, and these theories might be the most appropriate ones to apply for this dataset.

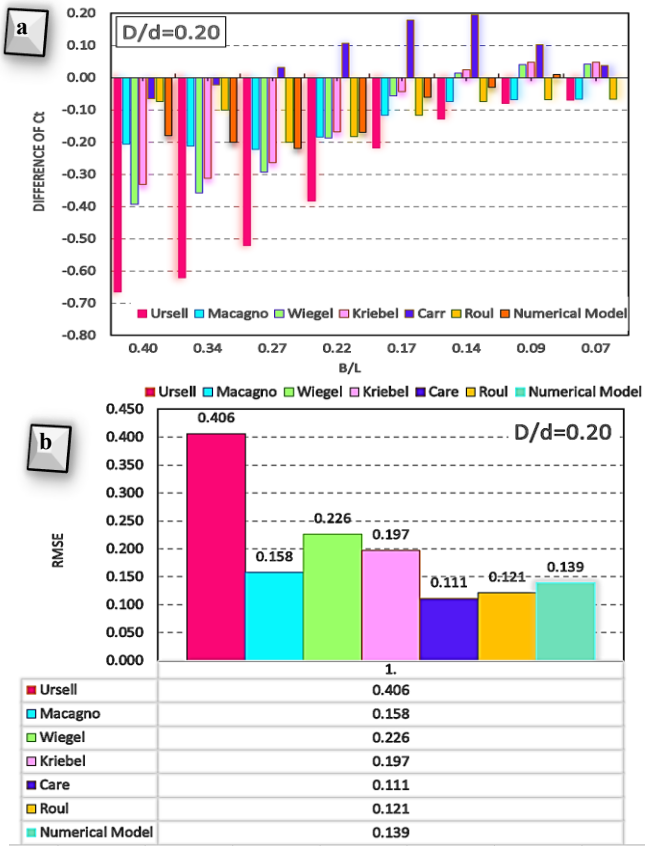

Figure 14: (a): Differences of the C_t between theories and the experimental data, (b): RMSE between theories and the experimental data in case of pile- restrained FB

Also, for the FB anchored by pile it is recommended to use the dimensionless parameter DB/L^2 to compare the transmission coefficient of floating breakwaters. The data for this type of FB under regular waves and D/d=0.2 is shown in the Figure 15. it is obvious that data for this type of breakwater distributed in a narrow band and there is no significant disparity.

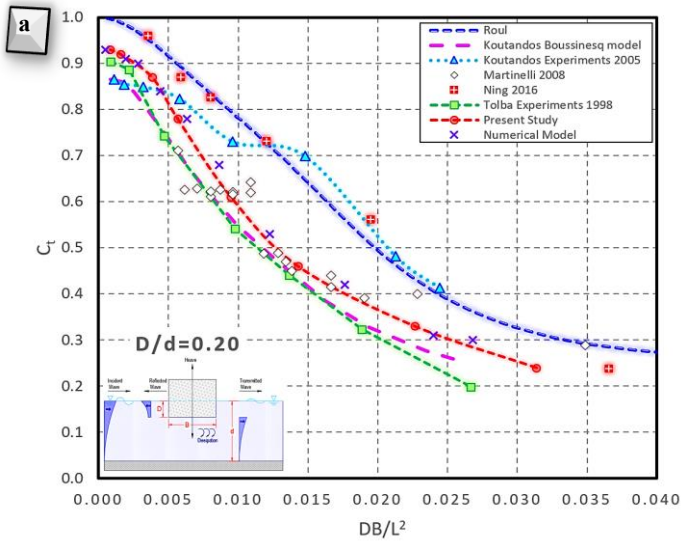

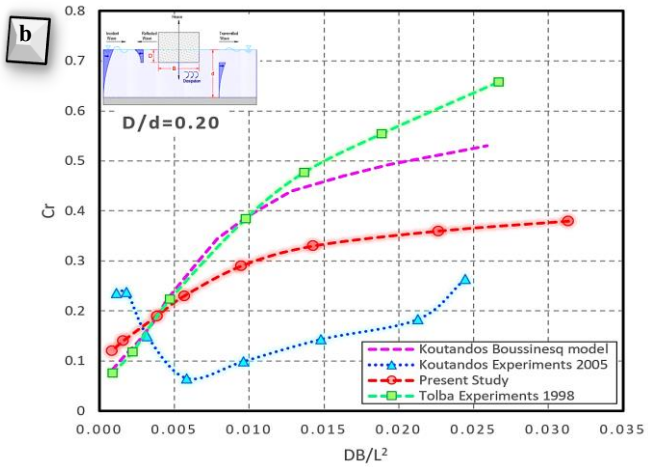

Figure 15: a: Transmission coefficient (C_t) variation against DB/L^2 parameter, b: Reflection coefficient (C_r) variation against DB/L^2 parameter – Pile-restrained FB

All the theories used for the comparisons with experimental data are derived for fixed structures, and a poor agreement is found for floating breakwaters with one degree of freedom. As it can be seen from Figure 13 and Figure 15, the relative period χ and dimensionless parameter DB/L^2 are two appropriate values to set on the x-axis for efficiency comparison of floating breakwaters anchored by pile. These two mentioned ratios contain all the parameters which influence the wave transmission coefficient.

3.1.3. Floating breakwater anchored by chain

For the FB anchored by chain, there are six degrees of freedom. Since all tests are conducted in the two-dimensional flume, there are three degrees of freedom, which are heave, sway, and roll. Chains were in loose condition and had submerged weight of 259 *g/m*. Their length was 3.35*m*, i.e., five times the water depth.

Ruol et al. [2013b] investigated the ranges of χ and D/d in which their formula would be applicable. They concluded that for χ-values between 0.5 and 1.5 and for D/d-values between 0.20 and 0.60, their formula is suitable to apply for both π-type and pontoon-type floating breakwaters. When the data of Brebner and Ofuya was compared with the formula of Ruol et al. a good agreement was found between the experimental data and the predicted values [12].

Martinelli et al. performed experiments in a flume (two-dimensional) and performed experiments in a basin (three-dimensional). Both experiments were performed with a D/d ratio equal to 0.13. For the two-dimensional dataset, a good agreement was found for the theory of Macagno. For the three-dimensional dataset, a good agreement was found for the theory of Ruol et al. and the wave transmission coefficients for this dataset are smaller than for the two-dimensional dataset. In this section only two-dimensional datasets are considered and therefore the three-dimensional dataset is neglected here [6].

Results related to the transmission coefficients of the incident waves on the model compared with the other research are presented in Figure 16.

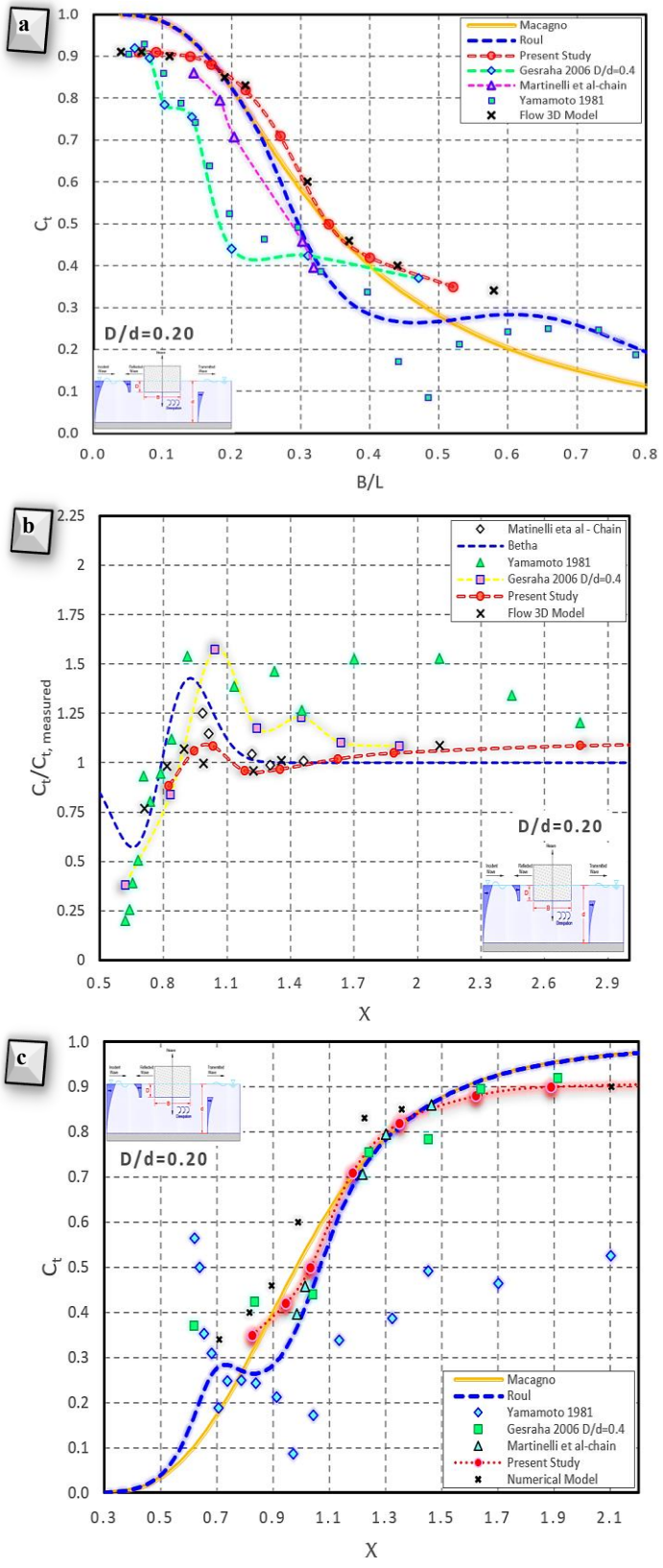

Figure 16: Comparison between theories and the experimental data – For the FB anchored by chain;
(a): Variation of transmission coefficient (C_t) against *B/L*,
(b): Variation of ($Ct/C_{t,\ measured}$) against χ parameter,
(c): Variation of transmission coefficient (C_t) against χ

For the FB anchored by chain, the difference between each theory and experimental data point is plotted in Figure 17-b. The RMSE for each theory in comparison with this dataset is shown in Figure 17-a. From this figure and related table, the theory of Roul and Macagno has the smallest RMSE, and this theory might be the most appropriate one to apply for this dataset.

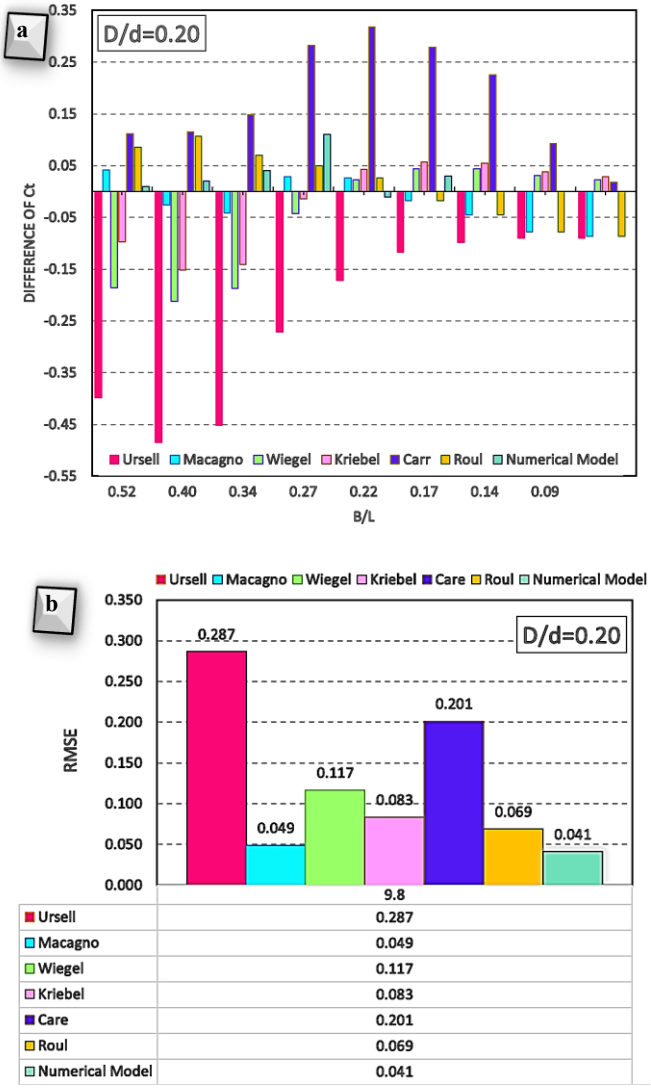

Ursell	0.287
Macagno	0.049
Wiegel	0.117
Kriebel	0.083
Care	0.201
Roul	0.069
Numerical Model	0.041

Figure 17: (a): Differences of the C_t between theories and the experimental data,
(b): RMSE between theories and the experimental data – The FB anchored by chain

In Figure 18, transmission coefficient (C_t) variation against DB/L^2 parameter is plotted for the FB anchored by chain under regular waves and D/d=0.2. As it is seen, the dimensionless parameter DB/L^2 is an appropriate value to set on the x-axis for floating breakwaters anchored by chain. This dimensionless parameter could gather all the datasets in a meaningful narrow band and decrease the disparity of data very well.

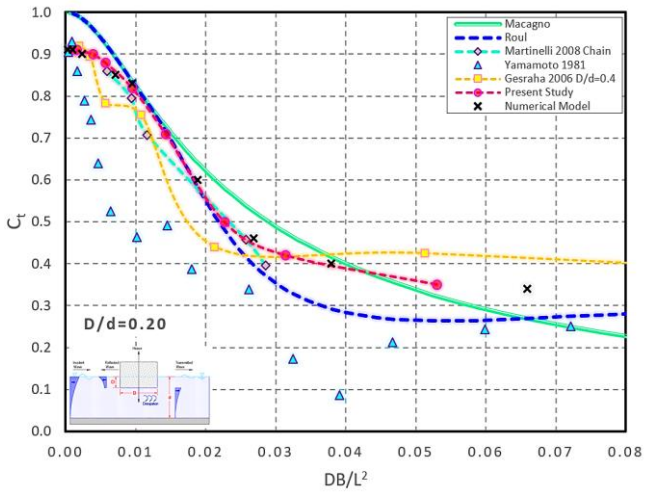

Figure 18: Transmission coefficient (C_t) variation against DB/L^2 parameter - FB anchored by chain

3.1.4. Floating breakwater anchored by tethered cable

As it has been mentioned above, there are also six degrees of freedom for the FB anchored by cable. In this case, the pretension cables were used as mooring lines. These mooring lines control the structure's movement to a considerable extent. Results related to the transmission coefficients of the incident waves on the model compared with the other research are presented in Figure 19.

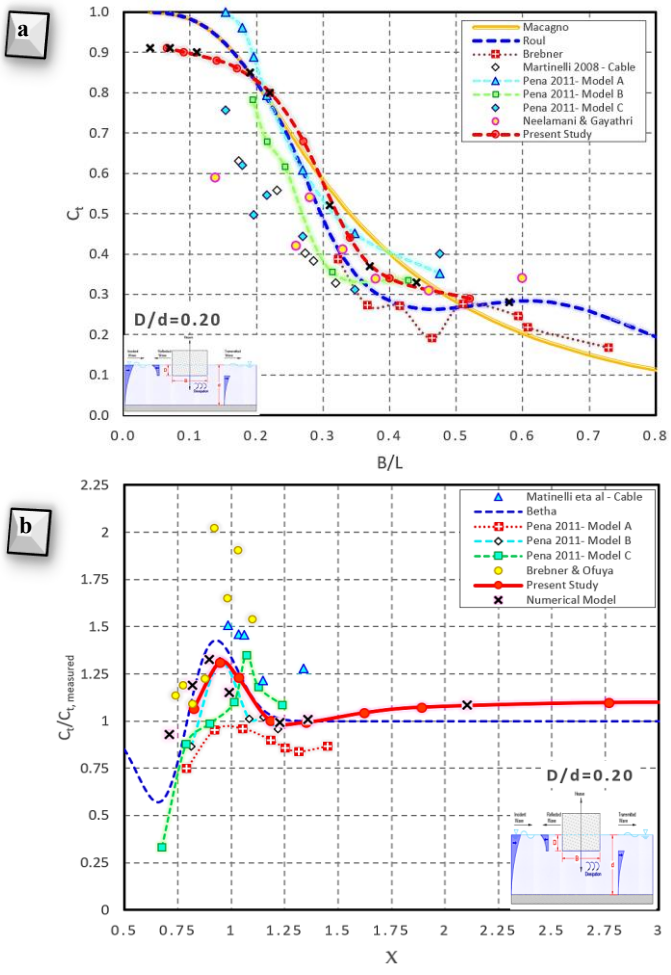

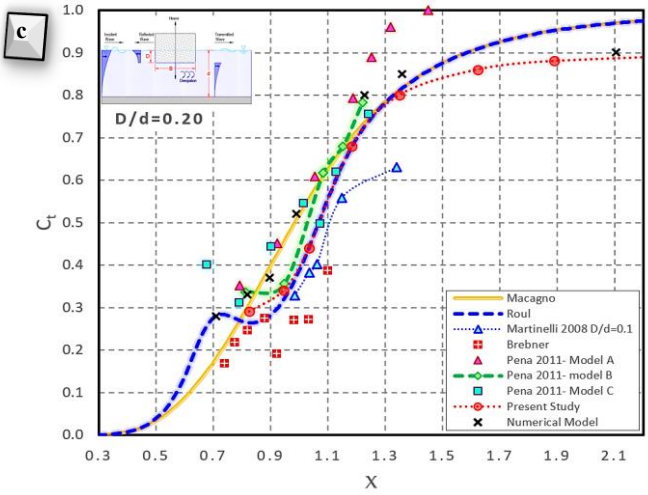

Figure 19: Comparison between theories and the experimental data -The FB anchored by tethered cable; (a): Variation of transmission coefficient (C_t) against B/L, (b): Variation of ($Ct\ /C_{t,\ measured}$) against χ parameter, (c): Variation of transmission coefficient (C_t) against χ

Figure 20-b shows the difference between each theory and experimental data point. The RMSE for each theory in comparison with this dataset is shown in Figure 20-a. From this figure, the theory of Roul and Macagno has the smallest RMSE, and this theory might be the most appropriate ones to apply for this dataset.

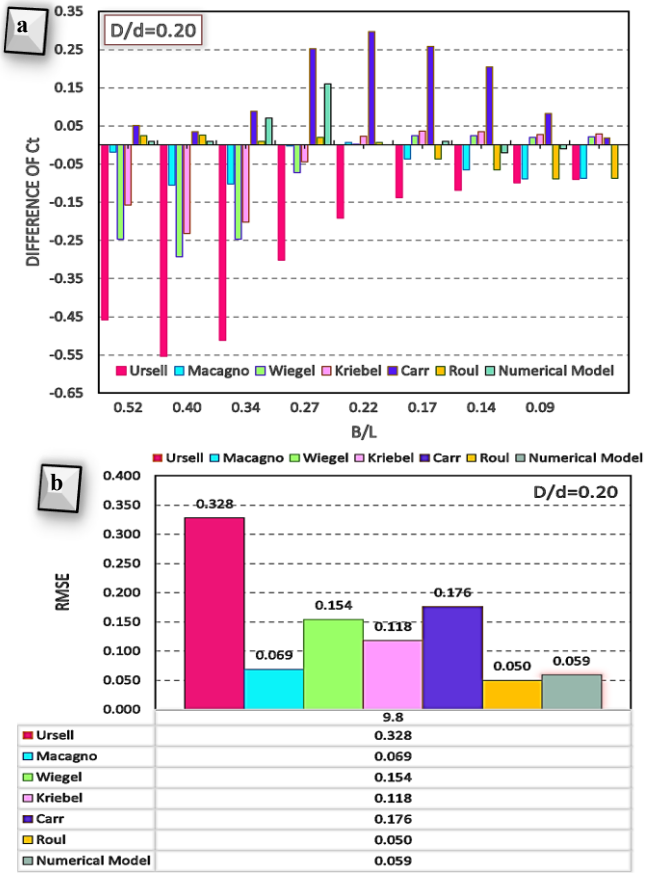

Figure 20: (a): Differences of the C_t between theories and the experimental data, (b): RMSE between theories and the experimental data -FB anchored by tethered cable

In Figure 21, the transmission coefficient (C_t) variation against DB/L^2 parameter is plotted for FB anchored by tethered cable under regular waves and D/d=0.2. As it is seen in this figure, the dimensionless parameter DB/L^2 is an appropriate value to be set on the x-axis for the floating breakwaters anchored by cable as well.

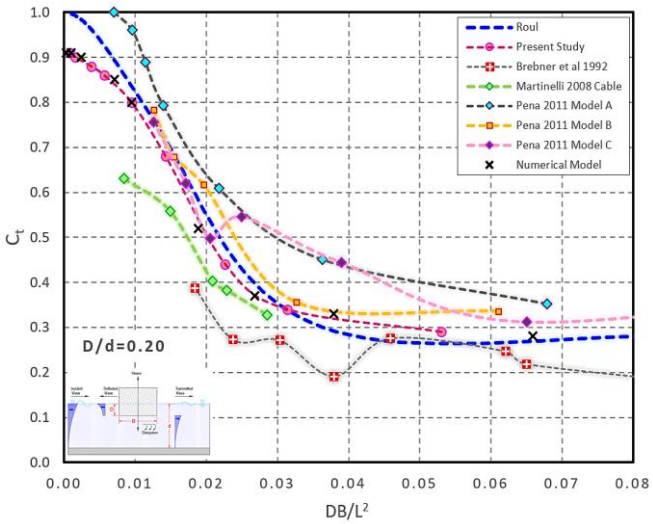

Figure 21: Transmission coefficient (C_t) variation against DB/L^2 parameter – The FB anchored by tethered cable

3.1.5. General comparative discussion

After a general review of each anchorage system and comparison of each one with previous research, the effect of the anchorage system on the transmission coefficient was compared with each other. Figure 22 shows the laboratory results obtained from the present study.

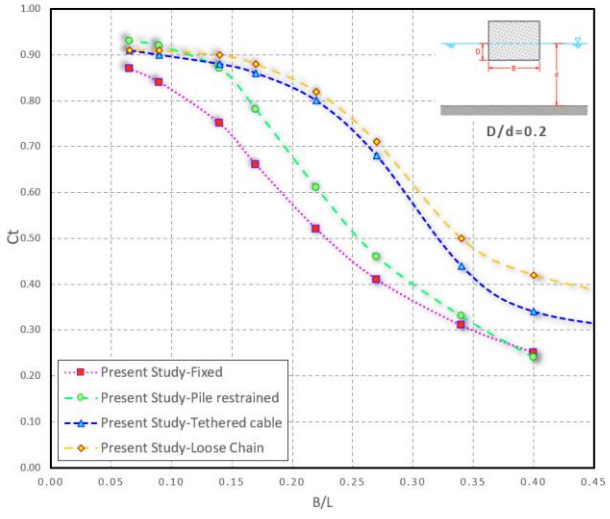

Figure 22: Comparison of the effect of anchorage system on wave transmission coefficient (C_t)

4. Conclusions

In this paper, a rectangular box floating breakwater was studied experimentally in four different FB configurations: (1) fixed breakwater, (2) pile-restrained (heave motion FB), (3) anchored by chain, and (4) tethered by elastic cable. In addition, the CFD method was used to study the mentioned configurations numerically. On the other hand, the effect of the draft of models were investigated. Based on deducted results, all the configurations were in acceptable range and had good agreements with previous investigation. According to Figure 22, the general results of the research are as follows:

1. For almost all wavelengths, the hydrodynamic behavior of the fixed breakwater was better than the other configuration.
2. Comparison of fixed breakwater with pile-restrained FB shows: In waves with short periods, the hydrodynamic behavior of breakwater with one-degree of freedom is almost very close to the fixed breakwater. For short wavelength, pile-restrained FB can have the same hydrodynamic behavior as the fixed one, even slightly better than it. This is due to the fact that when the breakwater located in the trough of the waves, Because of the heave degree of freedom the standing level of the breakwater is lower than the fixed type. When trough of waves is getting to turn to crest, because of wavelength shortness, there is not enough time that breakwater can match its standing level with the wave oscillations. Therefore, the breakwater has more draft in front of the waves and shows better performance than the fixed breakwater.
3. In high period waves (long waves), the hydrodynamic behavior of the pile-restrained FB is weaker than other configurations. This is due to the freeness of heave motion. In this configuration in the direction of heave, there is no movement restriction for the breakwater, so practically the breakwater mounts on the waves and shows the lowest efficiency.
4. Comparison of the breakwater anchored by cable with the breakwater anchored by chain shows: the effect of anchorage system's stiffness is more noticeable in waves with lower period, and since the chain has less restriction for displacement and the breakwater has more motion amplitude, its hydrodynamic performance is poor, so the wave transmission coefficient is higher. On the other hand, in waves with high period, the effect of stiffness of the anchorage system on the transmission coefficient is reduced.
5. Generally, the most efficient configuration was the fixed breakwater. However, regarding cost-effectiveness, the configuration of the FB with pile should be considered the most efficient for design purposes in mild conditions.

5. References

[1] McCartney, B.L., (1985), *Floating Breakwater Design*, Journal of Waterway, Port, Coastal, and Ocean Engineering, Vol.111(2), p.304-318.
[2] Biesheuvel A.C, (2013), *Effectiveness of floating breakwaters*, Msc Dissertation, Delf University of Technology.

[3] Mansard, E., and Funke, E., (1980), *The measurement of the incident and reflected spectra using the least squares method*, In: Proceedings of the 17th Coastal Engineering Conference ASCE, Sydney, p.154-172.

[4] Koutandos, E.V., Prinos, P., and Gironella, X., (2005), *Floating breakwaters under regular and irregular wave forcing: reflection and transmission characteristics*, Journal of Hydraulic Research, Vol.43(2), p.174-188.

[5] Ruol, P., Martinelli, L., and Pezzutto, P., (2013a), *Formula to predict transmission for π-type floating breakwaters*, Journal of Waterway, Port, Coastal, and Ocean Engineering, Vol.139(1), p.1-8.

[6] Ruol, P., Martinelli, L., and Pezzutto, P., (2013b), *Limits of the new transmission formula for π-type floating breakwaters*, Coastal Engineering Proceedings, Vol.1(33), p.47.

[7] Ursell, F., (1974), *The effect of a fixed vertical barrier on surface waves in deep water*, In Proc. Cambridge Philos. Soc, Vol.43, p.374-382.

[8] Macagno, E., (1954), *Wave action in a flume containing a submerged culvert*, La Houille Blanche.

[9] Pena, E., Ferreras, J., Sanchez-Tembleque, F., (2011), *Experimental study on wave transmission coefficient, mooring lines and module connector forces with different designs of floating breakwaters*, Journal of Ocean Engineering, Vol.38, p.1150-1160.

[10] Abul-Azm, A.G., Gesraha, M.R., (2000), *Approximation to the hydrodynamics of floating pontoons under oblique waves*, Journal of Ocean Engineering, Vol.27, p.365-384.

[11] Bettess, P., Liang, S.C., and Bettess, J.A., (1984), *Diffraction of waves by semi-infinite breakwater using finite and infinite elements*, International Journal for Numerical Methods in Fluids, Vol.4(9), p.813-832.

[12] Brebner, and Ofuya, A.O., (1968), *Floating breakwaters*, In Proceedings of 11th Conference on Coastal Engineering, p.1055-1094.

[13] Cox, R., Coghlan I., and Kerry, C., (2007), *Floating breakwater performance in irregular waves with particular emphasis on wave transmission and reflection, energy dissipation, motions and restraining forces*, Coastal Structures Conference, Venice.

[14] Kriebel, D.L., and Bollmann, C.A., (1996), *Wave transmission past vertical wave barriers*, In Coastal Engineering Conference, Vol.2, p.2470-2483.

[15] Gesraha, M.R., (2006), *Analysis of π-shaped floating breakwater in oblique waves: I. Impervious rigid wave boards*, Journal of Applied Ocean Research, Vol.28, p.327-338.

[16] Drieman, R., (2011), *Feasibility study on the use of a floating breakwater to protect a new artificial beach in Balchik, Bulgaria*, Msc thesis, Delft University of Technology.

[17] Fousert, M.W., (2006), *Floating breakwaters*, Msc thesis, Delft University of Technology.

[18] Hales, L.Z., (1981), *Floating breakwaters: State of the art literature review*, Technical report, DTIC Document.

[19] Dong, G.H., Zheng, Y.N., Li, Y.C., Teng, B., Guan, C.T., and Lin, D.F., (2008), *Experiments on wave transmission coefficients of floating breakwaters*, Journal of Ocean Engineering, Vol.35, p.931–938.

[20] He, F., Huang, Zh., and Wing-Keung Law, A., (2013), *An experimental study of a floating breakwater with asymmetric pneumatic chambers for wave energy extraction*, Journal of Applied Energy, Vol.106, p.222-231.

[21] Ji, Ch., Cheng, Y., Cui J., Yuan, Zh., and Gaidai, O., (2018), *Hydrodynamic performance of floating breakwaters in long wave regime: An experimental study*, Journal of Ocean Engineering, Vol.152, p.154-166.

[22] Liu, Zh., Wang, Y., Wang, W., and Hua, X., (2019), *Numerical modeling and optimization of a winged box-type floating breakwater by Smoothed Particle Hydrodynamics*, Journal of Ocean Engineering, Vol.188, p.106246.

[23] Williams, A.N., Lee, H.S., and Huang, Z., (2000), *Floating pontoon breakwaters*, Journal of Ocean Engineering, Vol.27, p.221-240.

[24] Harms, V.W., (1979), *Data and procedures for the design of floating tire breakwaters*, Water Resources and Environmental Engineering Rep, No.79-1, Dept of Civil Eng., State University of New York at Buffalo.

[25] Harms, V.W., Westerink, J.J., Sorensen, R.M. and McTamany, J.E., (1982), *Wave transmission and mooring force characteristics of pipe-tire floating breakwaters*, Technical Paper No. 82-4, US. Army, CERC.

[26] Carr, J.H., (1951), *Mobile Breakwaters*, Proceeding of the Second Conference on Coastal Engineering, Vol.28(1), p.281-295.

[27] Yamamoto, T., (1982), *Moored floating breakwater response to regular and irregular waves*, Journal of Applied Ocean Research, Vol.3, p.114-123.

[28] Yamamoto, T., Yoshida, A., and Ijima, T., (1980), *Dynamics of elastically moored floating objects*, Journal of Applied Ocean Research, Vol.2, p.85-92.

[29] Mohammd-Beigi.K, M., Kazeminezhad, M.H., Yeganeh-Bakhtiary, A., (2018), *Numerical Study on Hydrodynamic Force and Wave Induced Vortex Dynamics around Cylindrical Pile*, IJCOE, Vol.3, No.4, p.1-11.

[30] Zabihi, M.K.Kh., Mazaheri, S., Rezaee Mazyak, A., (2017), *Wave Generation in a Numerical Wave Tank*, IJCOE, Vol.2, No.4, p.33-43.